Article

Significant contribution of fractal morphology to aerosol light absorption in polluted environments dominated by black carbon (BC)

Check for updates

Baseerat Romshoo [1,2] ✉, Thomas Müller[1], Ajit Ahlawat[1], Alfred Wiedensohler[1], M. V. Haneef[3], Mohd. Imran[3], Aisha Baig Warsi[3], Anil Kumar Mandariya [4], Gazala Habib[3] & Mira L. Pöhlker[1,2,5]

In recent years, researchers have emphasized the use of fractal aggregate morphology instead of the core-shell morphology in global climate models for estimating black carbon (BC) forcing. This study confirms that fractal morphology plays an important role in reducing the overestimation of aerosol light absorption calculations in the case of an urban polluted environment. During periods of high anthropogenic BC emissions at Delhi, the particle light absorption is overestimated by 50 to 200% by assumptions of both external mixing and internal core-shell mixing. While incorporating the aggregate morphology model into light absorption simulations is beneficial in such cases, it comes with a high computational burden. To address this, we propose a metric known as morphology index (MI). This index distributes the weightage between the two extreme cases of core-shell and fractal aggregate to obtain accurate particle light absorption. Long-range transported aerosols were estimated to have an MI of 0.78, and fresh local emissions had an MI of 0.48. A BC-based aerosol classification approach was developed to determine the most relevant particle size mode for light absorption. The method is based on patterns found between the correlations of the BC mass concentrations and aerosol number concentrations at the different particles sizes (BC-size correlation spectra). BC-size correlation spectra are introduced as a concept that may be used (i) independently to understand the size-dependent heterogeneous distribution of aerosol light absorption and (ii) in conjunction with MI to accurately model the optical properties of aerosols in different BC regimes.

Black carbon (BC) is one of the main contributors to global warming and one of the biggest sources of uncertainty in radiative forcing estimates[1]. Global climate models (GCMs) typically assume that BC is internally mixed with sulfates and organics as homogeneous or core-shell (CS) spherical particles without taking into account the complex BC morphology[2-4]. There are certain GCMs that also assume a mixture of externally and simplified internally mixed BC aerosols[5,6]. Due to this simplified assumption of BC mixing state, radiative forcing calculations are subject to uncertainty[7,8].

A critical aspect that has been overlooked when adjusting the mixing state has been the fractal morphology of BC-containing particles, which can remain intact after being transported 500-1000 km from the emission source[9]. Recent studies have recommended incorporating more detailed assumptions concerning the mixing state into the current simplified core-shell model[10-12]. Laboratory-based studies have shown that the discrepancy in the modeled light absorption for laboratory-generated BC aerosols reduces significantly when a fractal aggregate assumption is used[13,14]. The BC fractal morphology, however, has been reluctant to be adapted as there is a limitation on their use due to their computationally costly simulations. Numerical studies have developed parametrization schemes and databases using fractal morphology to predict their light absorption and subsequent radiative effects[15-17].

[1]Leibniz Institute for Tropospheric Research, Leipzig, Germany. [2]Multiphase Chemistry Department, Max Planck Institute for Chemistry, 55128 Mainz, Germany. [3]Indian Institute for Technology New Delhi (IIT-D), New Delhi, India. [4]Univ Paris Est Creteil and Université Paris Cité, CNRS, LISA, F–94010 Créteil, France. [5]Faculty of Physics and Earth Sciences, Leipzig Institute for Meteorology, Leipzig University, 04103 Leipzig, Germany. ✉e-mail: baseerat@tropos.de

Despite this, it remains important to address two aspects of including the complex mixing state of BC in GCMs: the first is to quantify particle light absorption by ambient BC-containing aerosols using fractal morphology, while the second is how to include the computationally expensive fractal BC simulations in GCMs. To answer these questions, it is crucial to conduct research in regions with high anthropogenic BC emissions, such as North China, India, and Southeast Asia, where BC represents a significant proportion of total aerosol emissions[18]. In order to account for the complex BC mixing states, it is necessary to develop a simplified metric for assigning weightage to aggregate morphology in conjunction with the contribution of the core-shell model without conducting fractal optical simulations from scratch.

Even though incorporating aggregate morphology into simulations for light absorption is intuitively beneficial, applying it to a mixed ambient aerosol population of fresh, semi-aged, and aged particles is challenging. Aerosol samples collected in the urban area of Beijing and the suburban area of Xianghe in China indicated that BC particles were a mixture of partially coated and fully embedded fractal aggregates[19]. The next challenge is to define a morphology metric for such variable atmospheric conditions with variable BC characteristics. Previous studies have shown how to apply heterogeneity in BC mixing states using relationships derived from single-particle soot photometers (SP2)[11,12]. Our study introduces the concept for guiding heterogeneous BC properties based on correlations between BC light absorption and particle size. Correlations that provide hints about BC characteristics can be used together with morphology metrics to provide GCMs with a way to incorporate the complex mixing state of BC.

For reducing the overestimation of aerosol light absorption calculations in urban polluted regions with high anthropogenic BC emissions, we confirm that fractal morphology is essential. Our case study shows that both external mixing and internal core-shell mixing assumptions can overestimate particle light absorption under high BC mass concentrations. While incorporating the aggregate morphology model into light absorption

simulations is beneficial in such cases, it comes with a high computational costs. To address this challenge, we propose a metric known as "morphology index". This index distributes the weightage between the two extreme cases of core-shell and fractal aggregate to obtain accurate particle light absorption. This study is introduces the concept of MI and BC-size correlation spectrums to the scientific community. The MI values are tabulated for different BC-size correlation spectra found in Delhi in an urban polluted environment.

Results
Study site
The atmospheric BC-containing aerosols were sampled at the Indian Institute of Technology Delhi (IITD) in New Delhi, India. An urban residential area surrounds the IITD campus, and the nearest source of local traffic emissions is a busy highway 150 meters away. The BC concentrations in New Delhi reach their highest levels during the Winter season, with a seasonal average of 25 $\mu g\,m^{-3}$ [20]. Therefore, the measurements were conducted in late Winter of 2020 between 20th February and 11th March. The geographical map of the study site and the surrounding conditions are shown in Supplementary Fig. 1. Detailed measurement results, meteorological conditions, and 72-h backward trajectory analysis are also presented in the Supplementary Results (Figs. S2–S7).

Modeled light absorption for ambient aerosols (simplified vs. "realistic" approach)
To calculate the aerosol light absorption, information from field measurements was used, along with assumptions regarding external or internal mixing of the BC and BC-free particles (Fig. 1). The time series comparing the observed absorption coefficient (σ_{abs}^{obs}) with the modeled absorption coefficient using external mixing ($\sigma_{abs}^{mod-Ext}$) is shown in Fig. 2a. The figure also compares the modeled absorption coefficient under two assumptions of
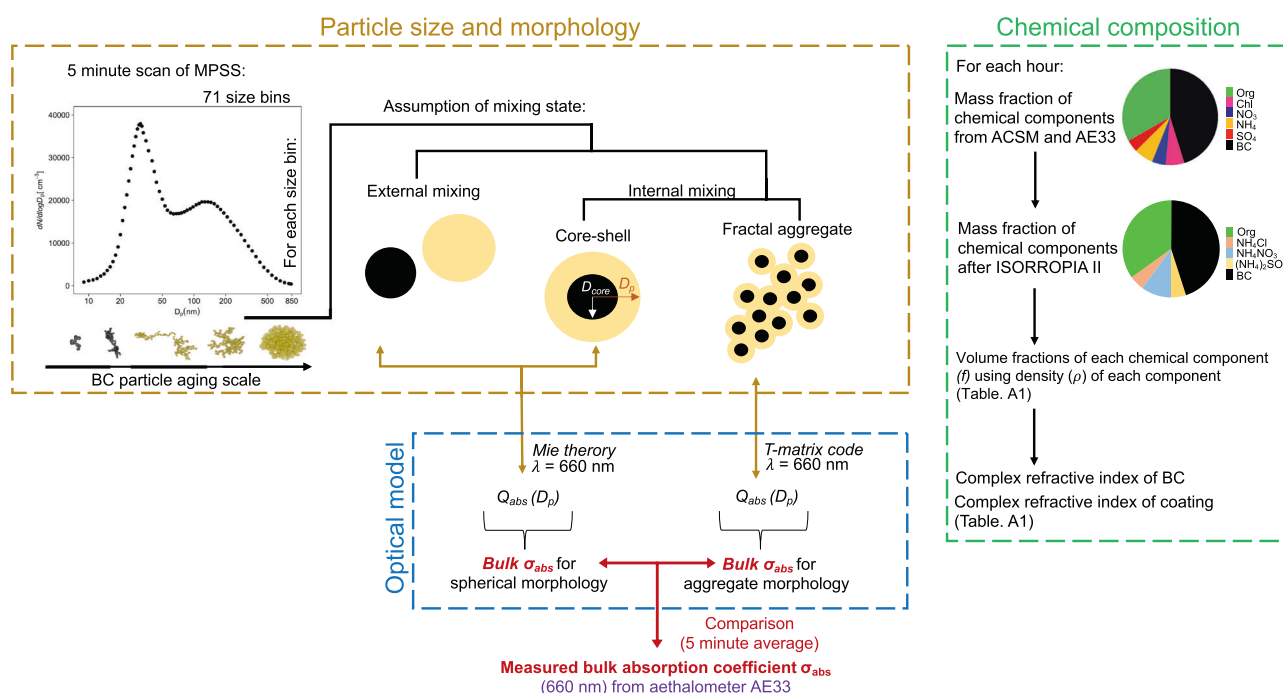

Fig. 1 | Schematic showing the prerequisites for modeling light absorption by BC-containing aerosols. Particle light absorption was modeled using five-minute scans of PNSD data under three different assumptions of mixing state: external mixing, internally mixed core-shell morphology and the internally mixed fractal-aggregate morphology. From the data obtained from the ACSM and AE33, the hourly volume fractions and complex refractive index of each chemical component are calculated.

Finally, optical models derive the modeled bulk absorption coefficient ($\sigma_{abs-mod}$) from the information provided regarding particle size, morphology, and chemical composition. The $\sigma_{abs-mod}$ is compared to the observed bulk absorption coefficient from the aethalometer ($\sigma_{abs-obs}$). The *Methods* section provides a more detailed description of the above modeling methodology.
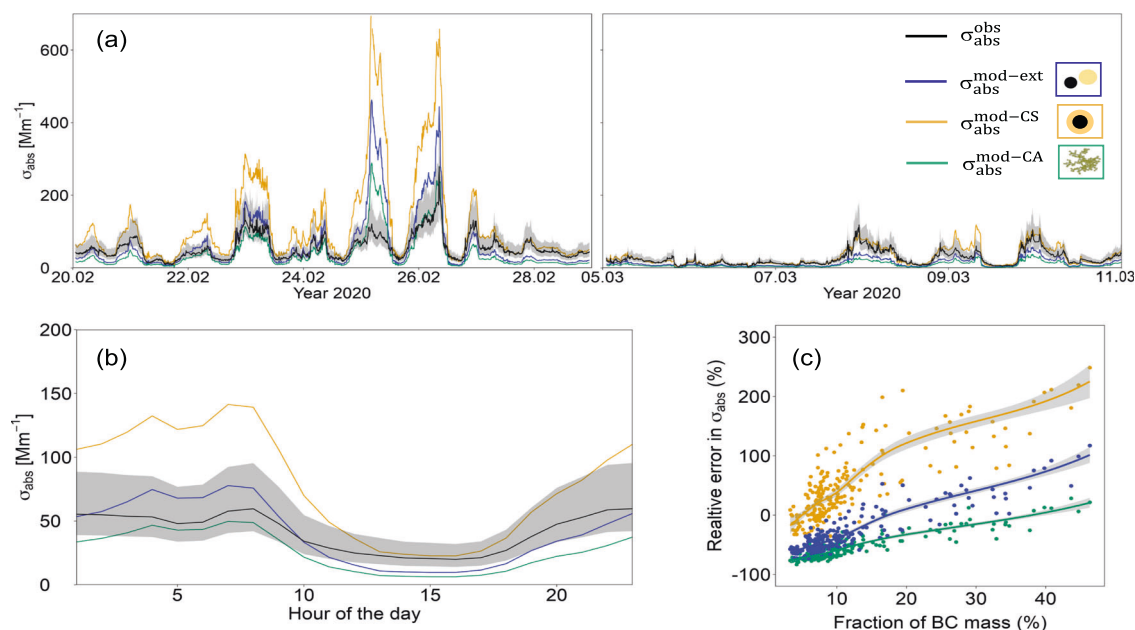
Fig. 2 | Comparison of the observed and modeled σ_abs at 660 nm. a Time series of the observed absorption coefficient (σ_{abs}^{obs}), the modeled absorption coefficient using the external mixing ($\sigma_{abs}^{mod-ext}$), the modeled absorption coefficient using the core-shell morphology (σ_{abs}^{mod-CS}) and modeled absorption coefficient using the coated-aggregate morphology (σ_{abs}^{mod-CA}). The grey area in **a** and **b** corresponds to the uncertainty in the AE33 when compared to reference instruments like multi-angle absorption photometer (MAAP); details can be seen in *Methods*. **b** Diurnal variation of the modeled and observed absorption coefficient. **c** Relative error in the modeled light absorption as a function of the fraction of BC mass (f_{BC}).

internal mixing, the core-shell morphology (σ_{abs}^{mod-CS}) and the coated-aggregate morphology (σ_{abs}^{mod-CA}).

There were significant periods during which the σ_{abs}^{mod-CS} was overestimated due to a larger absorption enhancement factor attributed when assuming non-spherical aerosols to be spherical[10,21]. On certain days at Delhi, the σ_{abs}^{mod-CS} was overestimated by more than 200%. On the contrary, the σ_{abs}^{mod-CA} was underestimated due to a comparatively lower absorption enhancement factor and a lower mass absorption cross-section of the non-spherical coated-aggregates[14]. Previous studies have corrected the overestimation by core-shell model with assumption of external mixing[10]. At a site with high levels of anthropogenic pollution, such as Delhi, the external mixing assumption also underestimated particle light absorption. When particle-to-particle heterogeneity is considered, the overestimation of particle light absorption is reduced by approximately 2–30%, depending on whether the atmospheric conditions are clean or polluted.[11,12] However, the largest deviation to the light absorption in this case was observed when assuming the fractal aggregate morphology of BC.

Comparison of σ_{abs}^{obs} with the modeled absorption coefficients ($\sigma_{abs}^{mod-Ext}$), (σ_{abs}^{mod-CS} and σ_{abs}^{mod-CA}) showed a diurnal variability (Fig. 2b). The σ_{abs}^{mod-CS} was in good agreement with σ_{abs}^{obs} during daytime. The agreement between the spherical core-shell morphology improved with increasing mass concentrations of organics (m_{org}). The slope between σ_{abs}^{obs} and σ_{abs}^{mod-CS} decreases from 3.04 to 1.44 as m_{org} exceeds 50–60 $\mu g \, m^{-3}$, (Supplementary Fig. 9). The better performance of the core-shell model in the presence of m_{org} is attributed to the growth mechanism of aerosols. In the presence of higher concentration of organic matter, a greater mass of condenses on BC particles and forms spherical structures, thus mimicking the core-shell structure. During the periods with m_{org} exceeding 50 $\mu g \, m^{-3}$, positive matrix factorization (PMF) analysis of organics measured by the Aerosol Chemical Speciation Monitor (ACSM) indicated that 60% of organics were from less oxidized (LOOA) and more oxidized (MOOA), suggesting secondary formation. The temporal variability of the sources of Organic Aerosols (OA) from positive matrix factorization (PMF) is illustrated in Supplementary Fig. 2.

However, during night-time and early morning, the σ_{abs}^{mod-CS} was overestimated by up to a factor of three. The largest overestimation of σ_{abs}^{mod-CS} during night-time was observed in the fourth week of February (23rd to 26th of February), where we also observed a higher mass fraction of BC (f_{BC}). The σ_{abs}^{mod-CA} showed a good agreement for periods when the core-shell model performed poorly. This polluted period was characterized by elevated levels of NO emissions (Fig. S4), indicating fresh BC from vehicular emissions[22]. The dominance of fresh vehicular emissions with a fractal morphology during this period explains the observed good agreement between σ_{abs}^{obs} and σ_{abs}^{mod-CA}. Furthermore, the comparatively lower wind speed during this period (Fig. S6) favored the accumulation of pollutants from the local sources[23,24].

There was a significant influence of f_{BC} on the comparison of observed and modeled light absorption coefficients. The dependence of the relative errors in the modeled light absorption on f_{BC} is shown in Fig. 2c. The result shows that the relative percent error (Eq. 7) due to the external mixing assumption is small when f_{BC} is less than 10%. When the f_{BC} exceeds 10% in urban polluted regions, the external mixing assumption and internally mixed core-shell assumption resulted in large relative errors of 50–200%. Overall, the two extreme cases of the spectrum are represented by the core-shell and coated aggregate models of internal mixing. These cases can be used as surrogates for modeling the light absorption of BC-containing aerosols. The performance of the coated-aggregate and core-shell model for different scenarios of f_{BC} has been shown in Supplementary Fig. 8.

Morphology index (MI) as a metric for correcting overestimation in particle light absorption

A singular morphology assumption falls short of providing accurate results when modeling light absorption by BC-containing aerosols. Incorporating the aggregate morphology model for the light absorption simulations, however, entails a significant computational burden. To address this challenge, we propose a metric that assign weightage to aggregate morphology in conjunction with the contribution of core-shell models, when applicable. This metric is referred to as the morphology index MI. A synonymous term for MI is the 'fraction of core-shell model ($f_{core-shell}$)'. Determining of MI involves an empirical parametrisation of the morphology-resolved particle light absorption, detailed in *Methods*.
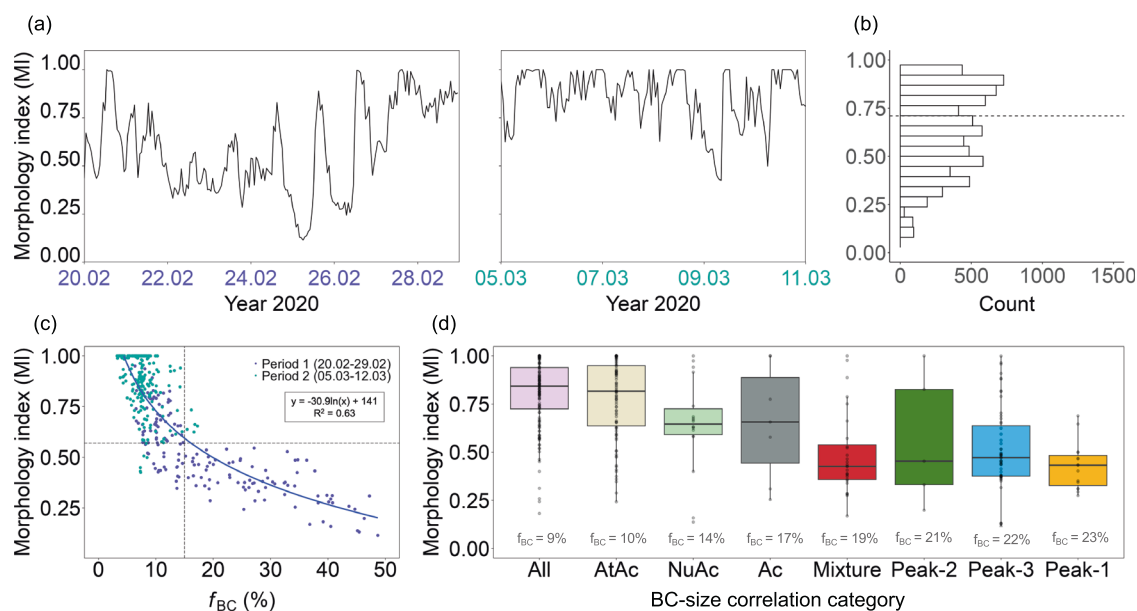
Fig. 3 | Morphology index (MI) for accurately modeling σ_{abs}. a Time series showing the values of the MI that was used for the prediction of $\sigma_{abs\text{-}obs}$. **b** Distribution of the MI during the entire measurement period with a median MI of 75 indicated by the dashed line. **c** Correlation between the MI values and the f_{BC}. The first six days of the campaign marked in purple **and t**he rest days of the campaign marked in bluish-green, indicated along on the X-axis of **a. d** shows the variation in the MI as a function of eight types of categories in the BC-size correlation spectrum.

In this study, the MI was calculated for an urban environment characterized by periods of strong influence from fresh local emissions and another period marked by influence from aged, long-range transported particles. The MI value represents the weightage assigned to the core-shell model, while the remaining 1-MI is the weightage given to the fractal aggregate model. As seen in Fig. 3a, the MI varied from 0.1 to 1 throughout the measurement periods. Notably, a median MI value of 0.75 was observed throughout the measurement period, as shown in Fig. 3b. For 16% of the total measurement period, we found a mean residual value of 0.26.

Identification of specific indicators in the atmospheric aerosols is essential for implementing the MI. BC-containing aerosols hold most relevance in the concept of MI because of their ageing process that profoundly influences the overall aerosol morphology. Figure 3c shows the distribution of morphology index (MI) values with respect to the measured f_{BC}. It was observed that there were two distinct periods with different dominant sources of aerosols during the campaign. In period 1 (20.02–29.02) where the local emissions dominated showed higher f_{BC} and consequently lower MI values (lower contributions of core-shell model). Period 2 (05.03–12.03) where the long-range transport dominated showed comparatively lower f_{BC} and higher MI values (higher contributions of core-shell model). The empirical distribution can be described by a collective lognormal fit. When the f_{BC} exceeds 15%, we observed an inversely relationship between the MI and f_{BC}. Conversely, for f_{BC} below 15%, the distribution is broader with a steeper slope. In this case, MI values suggest a BC-limited application, emphasizing the need to account for fractal aggregate morphology when BC concentrations are higher.

Categorization of the BC-size correlation spectrum

The characteristics of BC-containing aerosols can differ widely in the atmosphere[25]. For example, fresh aerosols containing BC emitted from diesel engines with peaks at 100–150 nm in the mass size distributions[26,27]. In contrast, the peak in the mass size distribution of aged BC occurs at sizes greater than 200 nm[28,29]. For our field measurements, the characteristics of BC-containing aerosols varied significantly with particle size and time. This was demonstrated by correlating the particle number concentrations in each size bin of the MPSS ($N_{D_p(i)}$) to the BC mass concentration (M_{BC}) for hourly subsets. The correlation coefficient is plotted with their respective $D_p(i)$, resulting in a BC-size correlation spectrum. Further details about the

algorithm to derive the BC-size correlation spectrums are discussed in the *Methods*. The nature of the BC-size correlation spectrum varied depending on the hourly subset selected, resulting in eight categories shown in Fig. 4a.

Climate models treat BC aerosols differently depending on the source of emission, residence time in the atmosphere, and presence of other aerosol types. Industrial BC is considered to be emitted into the atmosphere as externally mixed particles in the Aitken mode[2]. As the aerosol size increases larger than 0.1 μm in the accumulation mode, the BC is mostly considered to be mixed with sulfates and organics[3]. Other smaller particles from primary emissions coagulate with larger pre-existing particles and mainly move into the larger sized population. In the first four categories shown in Fig. 4a, i.e., Nucleation-Accumulation (NuAc), Aitken-Accumulation (AiAc), Accumulation (Ac), and All modes (All), the correlation with the BC mass concentration was dominant for larger particle within the accumulation mode. We observed that categories of NuAc, AiAc, Ac, and All modes dominated during the long-range transported events where BC is present in the accumulation mode along with Sulfates and Organics. The mean value of f_{BC} was 12% for these four long-range transport categories. High R^2 values for particles larger than 0.1 μm in these four categories indicates that the aged accumulation mode BC aerosols dominates the contribution to particle light absorption.

On the other hand, there are atmospheric conditions during which primary emissions dominate the aerosol load. This fresh local emission can be inferred from the narrow maxima of the high R^2 values towards the emission size range of aerosols. The four categories in the second row of Fig. 4a, i.e., Peak 1, Peak 2, Peak 3, and Mixture showed the highest correlation of BC mass concentration for sizes smaller than the accumulation mode particles. A particularly strong correlation of the BC with smaller particle sizes was observed for Peak 1, Peak 2, and Peak 3. During this time, the airmass is hypothesized to be predominant by a particular kind of local BC aerosol. The Peak 1, Peak 2, Peak 3, and Mixture categories are associated with fresh local emission conditions. The mean value of f_{BC} was 21% for the four categories of fresh local emissions. In these categories of local emission, the contribution of the smaller BC size modes to absorption is dominant, indicating the presence of fresh fractal BC. The time series of the different categories of the BC-size correlation spectrums throughout the measurement period is shown in Fig. 4b. The highest frequency among the BC-size correlation spectrums was of the All category which represents well-mixed
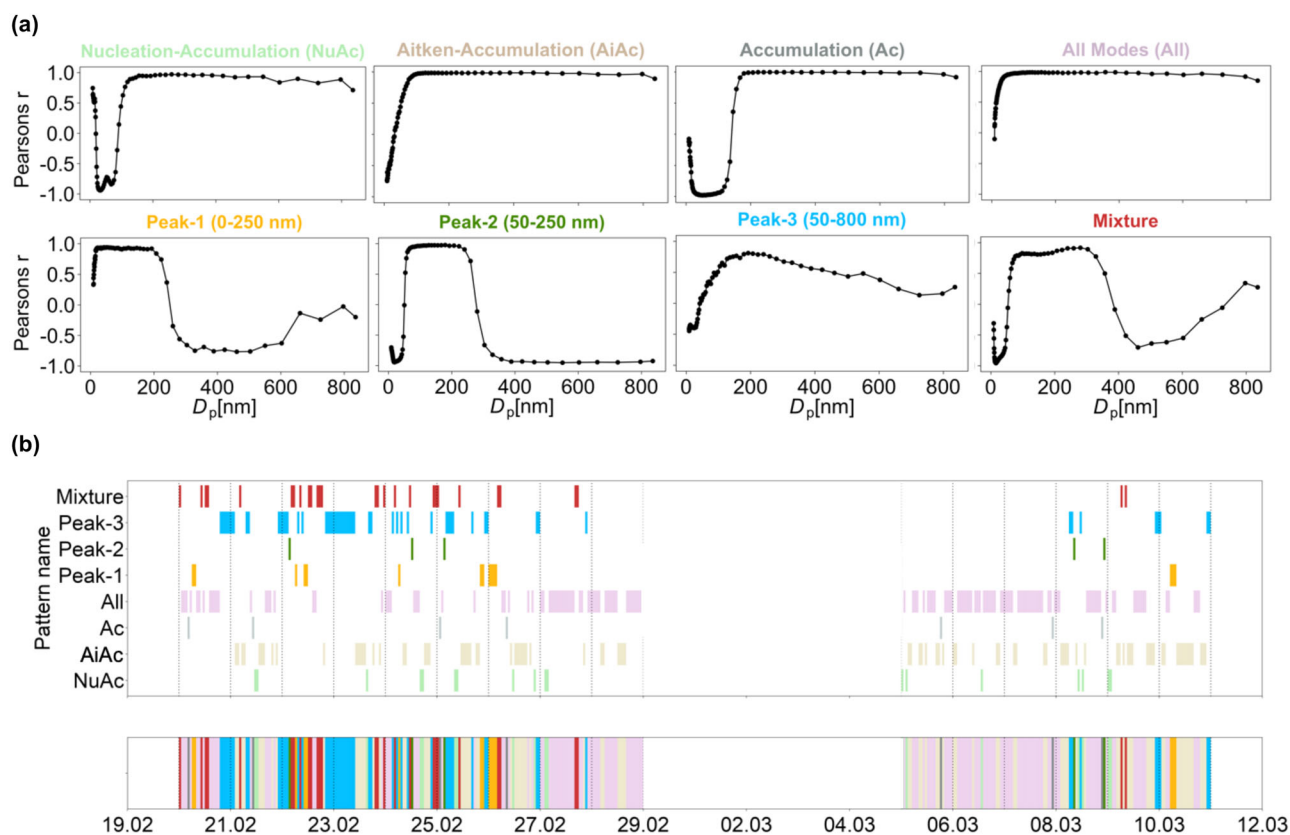
Fig. 4 | Categorization of the BC-size correlation spectrums. a Eight categories were identified in the BC-size correlation spectrums during the 15-day measurement period. The name of the BC-size correlation spectrum category is indicated at the top of each panel based on the particle modes in which the correlation coefficient was high. As part of the nomenclature of each category, a color is assigned to it, which is relevant to other results. **b** Time series showing the distribution of the different categories in the BC-size correlation spectrum across the measurement period. The colors of the segments follow the nomenclature given in **a**.

Table 1 | Classification of morphology index MI values are tabulated for different categories of BC-size correlation spectrums and their corresponding fraction of BC (f_{BC})

BC-size correlation spectrum	Fraction of BC (f_{BC})	Morphology index (MI)				Description	Mean MI[b]	Mean f_{BC}
		Median	25th	75th	Mean ± SD			
All	9	0.84	0.72	0.93	0.83 ± 0.17	Long range transport	0.78 ± 0.20	12
AiAc	10	0.81	0.63	0.94	0.83 ± 0.20			
NuAc	14	0.64	0.59	0.72	0.68 ± 0.23			
Ac	17	0.65	0.44	0.88	0.72 ± 0.29[a]			
Mixture	19	0.42	0.35	0.53	0.49 ± 0.21	Fresh local emissions	0.48 ± 0.18	21
Peak-2	21	0.45	0.33	0.82	0.62 ± 0.33[a]			
Peak-3	22	0.47	0.37	0.63	0.52 ± 0.21			
Peak-1	23	0.43	0.32	0.48	0.43 ± 0.12			

[a]less than 10 data points.
[b]excluding the Peak-2 and Ac spectrum due to sparse data points.
The MI values were separated into two categories of long-range transport and fresh local emissions, depending on the f_{BC} and BC-size correlation spectrum.

long range transported aerosols with homogeneous contribution to absorption at all particle sizes. Some of the categories closely resembled each other. For example, the Peak 2 resembles to the All. Similarly, the NuAC has a resemblance to the Ac. Consequently, Peak 2 and NuAc category had the lowest observations of less than 10 datapoints which caused higher uncertainties in their corresponding morphology index.

The link between BC-size correlation spectra and aerosol absorption simulations is established through the MI. These BC-size correlation spectra play an important role in implementing the MI to improve modeling of particle light absorption. Figure 3d shows the box-plot of the MI values with respect to the BC-size correlation spectra. The mean MI values observed for each category of BC-size correlation spectra is presented in Table 1. For the first four categories of the BC-size correlation spectra associated with long-range transport, the MI showed an average of 0.77, which means a 23% contribution of fractal aggregate morphology to the total light absorption. However, when the aerosols were dominant with fresh local emissions, the MI averaged a value of 0.51, indicating a 49% weightage to fractal aggregate morphology.

The improvement in the simulated light absorption of BC-containing particles when using the MI is demonstrated in Fig. 5. The time-series of the
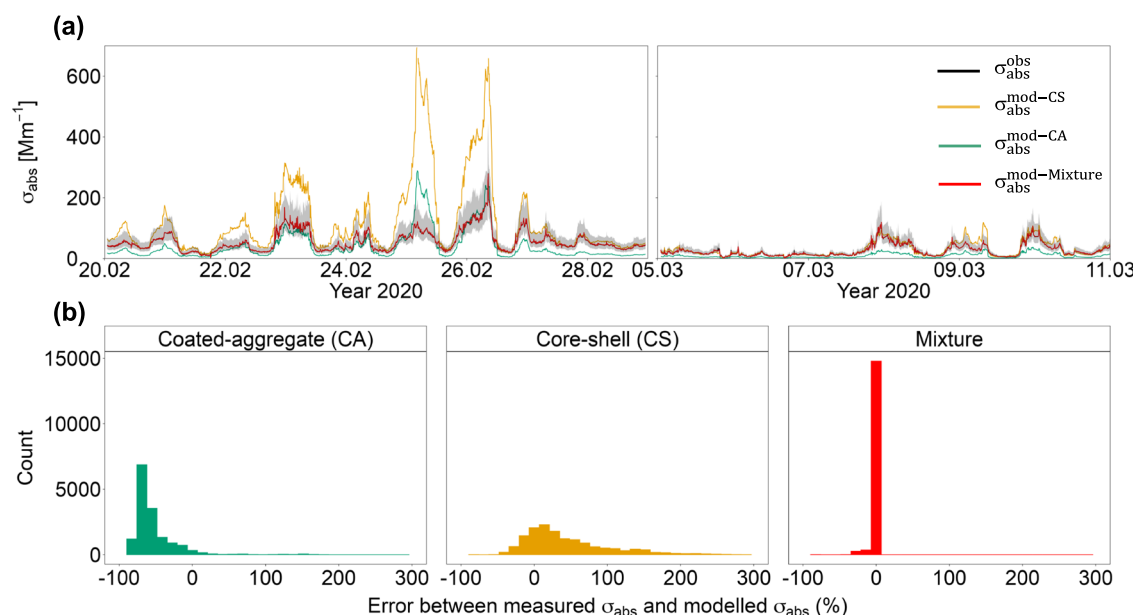
Fig. 5 | Improved modeled σ$_{abs}$ using morphology index. a Time series showing the absorption coefficient (σ$_{abs}^{mod-mixture}$) modeled using the morphology index added to Fig. 2a. **b** Comparison of the error distribution between modeled and measured absorption coefficient based on coated-aggregate morphology, core-shell morphology, and a mixture of both, i.e., using the morphology index (MI).

absorption coefficient (σ$_{abs}^{mod-mixture}$) shown in Fig. 5a derived by distributing the weightage between the two extreme cases of core-shell and fractal aggregate to match σ$_{abs}^{obs}$. The effectiveness of applying the MI is demonstrated by the error distribution between the modeled absorption coefficient and the measured absorption coefficient (Fig. 5b). The first two distributions are based on the conventional morphological assumption (i.e., coated-aggregate and core-shell morphologies). For coated aggregate morphology, the error distribution is narrowly concentrated in negative error percentages up to a maximum of −100%. The errors in the core-shell morphology are widely spread in the positive error ranges up to 200%. Finally, the third error distribution corresponds to when the morphology index was used to simulate light absorption, with the errors being very narrowly concentrated at zero percent, what is expected from our approach .

Discussion

This study demonstrates that the previously recommended methods for light absorption calculations involving external mixing or internal core-shell mixing are insufficient in a heavily polluted case like urban Delhi. In the presence of a higher concentration of organic matter, a greater mass of condenses on the BC seed particles to form spherical structures that resemble the core-shell structure. However, when anthropogenic BC emissions are higher, the use of fractal aggregate morphology is necessary to reduce the overestimation of aerosol light absorption calculations.

Incorporating aggregate morphology models into light absorption simulations in regions with high anthropogenic BC emissions is beneficial, but comes with a large computational cost. As a solution to this, we have proposed a metric known as the morphology index (MI). To obtain accurate particle light absorption, this index distributes the weight between two extreme cases of core-shell and fractal aggregate. A concept for guiding BC characteristics is presented as a correlation between BC and particle size. BC-size correlation spectra provide insights into the particle sizes where BC aerosols are dominant, serving as a useful guide for understanding BC characteristics. The MI values were tabulated for different categories of BC-size correlation spectrums representing long-range transported aerosols or local fresh emissions. A MI of 0.78 was obtained for long-range transported aerosols and a MI of 0.48 was found for local fresh emissions. Future work is required to test whether including the particle-to-particle

heterogeneity will reduce the mean residual value of 0.26 found during 16% of the total measurement period.

This study introduces the MI concept and BC-size correlation spectrums to the scientific community. The MI values are tabulated for different BC-size correlation spectra found in Delhi in an urban polluted environment. There is potential for developing the MI into a standard metric for morphological assumptions in climate models. This would improve predictions of direct radiative forcing. For this metric to be universally applicable, it must be tabulated for different atmospheric conditions or environments and implemented using certain indicators. Further research should be conducted involving more elaborate measurement campaigns to develop this concept that corrects aerosol light absorption simulations.

Methods
Instrumentation

The particle number size distribution (PNSD) was measured using a MPSS at 71 sizes with mobility diameters (D_p) ranging from 8 to 800 nm with a time resolution of 5 min[30]. BC mass concentrations were measured using a multi-wavelength aethalometer (AE33, Magee Scientific, Berkeley, CA). Another unit of AE-33 was present at a location 50 m away. Filter-based absorption photometers are associated with inherent variability in BC mass concentrations[31]. The light absorption coefficient was corrected for multiple scattering effects using the Aerosol, Clouds and Trace Gases Research Infrastructure (ACTRIS) recommended harmonization factor (H) of 1.76[32]. This H-value was calculated as an average from simultaneous AE33-MAAP measurements in rural and urban European sites; it is currently a recommendation from ACTRIS to the network associates. Furthermore, the uncertainties in light absorption coefficients due to fluctuations in H-factor varying between 1.1 and 2.5 have been accounted for[15].

Since the modeling experiments were conducted at 660 nm, a wavelength at which BrC makes a relatively minor contribution to light absorption. It is at shorter wavelengths, such as 370 nm, that BrC aerosols play a more crucial role. During the measurement period at the urban site, sources of BrC aerosols, such as forest, crop, and grass burning, were not predominant The Angström absorption exponent (AAE) was also employed to disentangle the contributions of BC and BrC to absorption. The mean AAE observed over the entire measurement period was 1.18. The temporal variability of the AAE is illustrated in the Fig. S1e.

Even though the developments reported in this study are related to BC aerosols, an Aerodyne Aerosol Chemical Speciation Monitor (ACSM, Aerodyne Research, Billerica MA) provided mass concentrations of organic matter (OM), ammonium (NH_4), sulfate (SO_4), nitrate (NO_3), and chloride (Cl). A detailed description of the ACSM setup is given in a previous study[33,34]. A positive matrix factorization (PMF) analysis of organic mass spectral data obtained from the Aerosol Chemical Speciation Monitor (ACSM) revealed that biomass burning organic aerosol (BBOA) had the lowest mean contribution at 15%.

Modeling light absorption of ambient aerosols
For modeling the optical properties of BC-containing particles, it is essential to consider three prerequisites, chemical composition, particle size, and morphology.

Chemical composition. The mass concentrations of BC and other chemical species were measured every hour by the AE33 and ACSM, respectively. The mass concentrations of the chemical compounds present in the aerosol particles were calculated from the mass concentrations of the chemical species by using an ion-pairing scheme ISORROPIA II at 293 K and 0% RH[35]. The volume concentrations of each chemical compound were calculated using their density (ρ), which can be found in Table S1. The volume fraction of each chemical compound (f_i) was thus determined, separating them into the volume fraction of BC (f_{BC}) and volume fraction of coating $f_{coating} = f_{OM} + f_{NH_4Cl} + f_{NH_4NO_3} + f_{(NH_4)_2SO_4}$.

The values of the complex refractive index for BC and organics, were assumed to be $2 + 0.63i$ and $1.47 + 0i$, respectively[36]. The complex refractive index of the coating was calculated using a volume mixing rule with the individual fractions of the chemical compounds excluding BC. The details about the complex refractive index of the other chemical compounds are given in Table S1. All refractive indices are provided for the wavelength 660 nm.

Particle size and morphology. The two most commonly used morphologies for internally mixed BC-containing aerosols were considered in this study. Among atmospheric scientists, the spherical core-shell model is the most commonly used because of its simplicity and versatility. In the spherical core-shell model, the BC consists of the inner core of particles surrounded by a coating (or shell) consisting of the remaining chemical components (Fig. 1):

$$D_{core}^3 = f_{BC} \cdot D_{shell}^3 \tag{1}$$

where D_{shell} is the diameter of the outer shell, D_{BC} is the dimeter of the inner BC, and f_{BC} is the fraction of BC. f_{BC} is derived from the mass concentrations of chemical components measured with the ACSM and AE33. Since we simulate the aerosol particles for each bin of the PNSD, the $D_{shell} = D_p$.

The fractal aggregate model represents the real morphology of BC aerosols, but it is more computationally expensive. In the fractal aggregate model, there are numerous primary particles that are individually coated (Fig. 1). A fractal aggregate equivalent to the D_m of each size bin in the MPSS is simulated using tunable diffusion-limited aggregation (DLA) software[37]. The number of primary particles (N_p) in the fractal aggregate is calculated from the measured mobility diameter D_m using the conversion given by:

$$D_m = a_o \cdot N_p^{0.46}, \quad N_p < 100 \tag{2}$$

$$D_m = a_o \cdot (10^{-2x+0.92}) \cdot N_p^x, \quad N_p > 100 \tag{3}$$

Where, a_o is the outer diameter of the primary particle, x is the mobility mass scaling exponent, $0.46 < x < 0.56$[38]. In this study, the average value of the mobility mass scaling exponent $x = 0.51 \pm 0.02$ was assumed.

The required input parameters for the DLA software are N_{pp}, a_{pp}, and D_f. The radius of the primary particle of a BC fractal aggregate is commonly polydisperse, varying within a narrow range of 10–25 nm[39]. However, the optical properties are insensitive to the change in the radii of the primary particle when in the range of 10–25 nm[40]. For the sake of simplicity, the a_{pp} is set to 15 nm[14,15].

The fractal dimension of BC particles is determined by the source of emission. Transmission electron microscopy (TEM) analysis showed that the fractal dimension of samples collected under different ambient conditions ranged between 1.8 and 2.16[41]. For freshly emitted wildfire carbonaceous particles, a D_f of 1.92 was measured near to the emission source[42]. For heavily coated BC-containing particles, the D_f can be as high as 2.8[43]. Some ambient studies have also reported D_f between 2.3 and 2.8[44]. This study considered 2.3 as average in the range of 1.5 to 3.0 (sphere) used in Mie calculations. Supplementary Fig. 10 illustrates a sensitivity study where the fractal dimension is varied between 1.7, 2.3 and 2.9, to also represent the two other cases.

Transmission electron microscopy (TEM) images from Shanghai's atmosphere showed a variety of semi-aged BC fractal aggregates that have a uniform or non-uniform coating comprising other chemical components around them[19]. Next, the fractal aggregate is coated using the closed-cell approach[45] following:

$$\frac{4}{3}\pi a_i^2 = f_{BC} \cdot \frac{4}{3}\pi a_o^2 \tag{4}$$

where a_i is the inner diameter of the primary particle. The realistic model when compared to the closed-cell model used in this study has shown good comparability[46].

Optical model. The particle light absorption was calculated for each size bin of MPSS after constructing the particles using information about particle size, chemical composition, and either of the three morphological assumptions. The Lorenz-Mie theory and the Multi-Sphere T-matrix Method (MSTM) code[47] were used to calculate the absorption efficiency Q_{abs} of aerosols having spherical and fractal morphologies, respectively. Then the absorption cross-section C_{abs} (in units of m^2) is calculated from the Q_{abs} for each D_{mi} as:

$$C_{abs}(D_{mi}) = Q_{abs}(D_{mi}) \cdot \pi \frac{d_{mi}^2}{4} \tag{5}$$

The bulk light absorption represented by the absorption coefficient σ_{abs} (unit: Mm^{-1}) is the sum of the absorption cross-section C_{abs_i} calculated for each diameter D_{mi} of the particle number size distribution (PNSD):

$$\sigma_{abs} = \sum_{i=1}^{n} C_{abs}(D_{mi}) \cdot N(D_{mi}) \tag{6}$$

MSTM simulations were conducted every five minutes for each of the 71 size bins and each morphology, yielding 8640 simulations (data points). If the particle size is 800 nm or larger, each fractal morphology simulation can take several hours, resulting in high computational costs.

The relative percent error in the modeled light absorption coefficient $\delta(\sigma_{abs})$ is calculated as:

$$\delta\sigma_{abs}(x) = \frac{|\sigma_{abs}^{obs} - \sigma_{abs}^{mod}(x)|}{|\sigma_{abs}^{obs}|} \times 100\% \tag{7}$$

where x is the assumption of external mixing, internally mixed core-shell and internally mixed coated aggregate.

BC-size correlation spectrum - correlations between particle size and BC mass concentration
Earlier studies have used clustering techniques to categorize the PNSD of aerosols according to their portions in various particle size ranges[48]. For

example, the PNSD of Artic aerosols were clustered and categorized into four types: Washout, Nucleation, Intermediate, and Polluted[49]. Further, different size ranges of the PNSD have been correlated to the BC mass concentration showing seasonal correlations[50]. This study investigated the hourly relationships between particle number concentrations in each size bin of the PNSD and BC mass concentrations. BC aerosols are typically small near the source of emission, primarily faling into the Aitken and nucleation size modes. However, it is possible to observe BC-containing aerosols in larger sizes up to 800 nm, either due to the agglomeration of smaller aggregates or the presence of other chemical constituents. A detailed discussion with examples of BC particles collected in different environments and with different shapes and sizes are given in the Supplementary to this work.

A sub-set of the MPSS and AE33 data is taken for each hour of the measurement period of 15 days. Within an hourly subset, the bulk BC mass concentrations are correlated individually with the $N(D_{mi})$ for each of the 71 size bins of the PNSD. From this correlation, the Pearson coefficient of determination (r) was noted for each particle size bin $D_m(i)$. The r_i derived for the 71 size bins are plotted with their respective $D_m(i)$, resulting in a BC-size correlation spectrum (Fig. S11). Depending on the selected hourly subset, the distribution of the r_i values with $D_m(i)$ varied, resulting in different BC-size correlation spectrums. Depending on the distribution of the r_i values with $D_m(i)$, the hourly BC-size correlation spectrums were assigned to eight categories shown in Table S2. The categorization was done manually and is, therefore not entirely objective. Analyzing data sets from other environments could lead to different categories and assigned spectra. The data for two consecutive hours were combined in certain BC-size correlation spectrums, where the r_i was low for the whole size range.

Morphology index (MI) for modeling light absorption of BC-containing particles

Black carbon is assumed as a homogeneous or core-shell (CS) spherical particle without considering their complex fractal morphology in GCMs such as in the aerosol-climate modeling earth system ECHAM5-HAM, or the Multiconfiguration Aerosol TRacker of mIXing state in the Goddard Institute for Space Studies climate model[2–4]. For example, in the GISS-MATRIX, the total aerosol loads show that the internal mixture between BC with organics and sulfates populations contain almost all BC in the atmosphere, which leaves 1% of BC in the atmosphere as external mixture[3].

To account for the fractal morphology of BC-containing particles, an empirical parametrisation is derived for the morphology-resolved particle light absorption for internally-mixed BC, which is represented as a central estimate σ_{abs} and a residual term ϵ:

$$\sigma_{abs}^{internally-mixed} = \sigma_{abs}^{CS} \cdot MI + \sigma_{abs}^{CA} \cdot (1 - MI) + \epsilon \quad (7)$$

The morphology-resolved particle light absorption is expressed as a weighted average between σ_{abs}^{CS}, the modeled absorption coefficient using the core-shell morphology, and σ_{abs}^{CA}, the modeled absorption coefficient using the aggregate morphology. Morphology index (MI) is the proposed metric used to accurately predict the particle light absorption by tuning the mixing state in terms of morphology i.e., the fraction of relatively fresh fractal aggregates amidst the total BC population.

There are certain models such as a Modal Aerosol Dynamics model for Europe including insoluble modes (MADE-in), consisting of seven modes characterized by particle size, composition and mixing state, was also developed[5]. In MADE-in, the BC aerosol is distributed in four modes, according to two sizes (Aitken mode and accumulation mode) and two BC mixing states (external and CS mixture).

In such cases of both external and internal mixtures of BC, the (Eq. 7) must be modified as:

$$\sigma_{abs} = \sigma_{abs}^{internally-mixed} \cdot IMI + \sigma_{abs}^{externally-mixed} \quad (8)$$

where IMI stands for the internal mixing index, and can be obtained from instruments such as SP2. The value of MI is bound to change subject to the

geographical site, meteorological conditions, and atmospheric chemistry. For our case study at an urban site, the two cases of internally mixed BC well represented the two extremes of the entire absorption spectrum, therefore the (Eq. 7) was sufficient to represent the observational absorption.

The uncertainty in the MI due to the uncertainties in the modeled absorption coefficient from measurement uncertainties. The measurements that were used as inputs for modeling the absorption coefficient are particle mobility diameter from the MPSS, and chemical composition from the AE33-ACSM measurements. The uncertainty in the particle mobility diameter from the MPSS is 2%[51], whereas the uncertainty in the BC mass fraction from the AE33-ACSM is nearly 20%[32,52]. Sensitivity analysis showed that the ± 20%, measurement uncertainty from the AE33-ACSM set-up results in a change of between ± 0.12 and ± 0.33 in MI. This uncertainty is primarily due to the artifacts of filter-based absorption instruments like AE-33. In future, in order to reduce this uncertainty, it is recommended to include results from EC-OC analysis of aerosols collected on filters. Further, laser incandescence-based instruments like single particle soot photometers (SP2) can be used to derive the observational mixing state.

Data availability
The data obtained from this study are available upon request from the corresponding author (baseerat@tropos.de).

Code availability
The software used to generate the fractal aggregates is available at https://sites.google.com/view/fabriceonofri/aggregates/fractal-like-aggregates-diffusion-model. The code used to model the optical properties of fractal aggregate; the multi-sphere T-matrix (MSTM) is publicly available at https://eng.auburn.edu/users/dmckwski/scatcodes/.

References
1. Wang, R. et al. Estimation of global black carbon direct radiative forcing and its uncertainty constrained by observations. *J. Geophys. Res. Atmos.* **121**, 5948–5971 (2016).
2. Bauer, S. E., Ault, A. & Prather, K. A. Evaluation of aerosol mixing state classes in the GISS modelE-MATRIX climate model using single-particle mass spectrometry measurements. *J. Geophys. Res. Atmos.* **118**, 9834–9844 (2013).
3. Bauer, S. E. et al. MATRIX (Multiconfiguration Aerosol TRacker of mIXing state): an aerosol microphysical module for global atmospheric models. *Atmos. Chem. Phys.* **8**, 6003–6035 (2008).
4. Stier, P. et al. The aerosol-climate model ECHAM5-HAM. *Atmos. Chem. Phys.* **5**, 1125–1156 (2005).
5. Aquila, V. et al. MADE-in: a new aerosol microphysics submodel for global simulation of insoluble particles and their mixing state. *Geosci. Model Dev.* **4**, 325–355 (2011).
6. Chen, G. et al. An aerosol optical module with observation-constrained black carbon properties for global climate models. *J. Adv. Model. Earth Syst.* **15**, 10 (2023).
7. Li, J. et al. Scattering and absorbing aerosols in the climate system. *Nat. Rev. Earth Environ.* **3**, 363–379 (2022).
8. Sun, J. et al. The chemical composition and mixing state of BC-containing particles and the implications on light absorption enhancement. *Atmos. Chem. Phys.* **22**, 7619–7630 (2022).
9. Sun, C. et al. Mixing state of black carbon particles in Asian outflow observed at a remote site in Taiwan in the Spring 2017. *J. Geophys. Res. Atmos.* **125**, 16 (2020).
10. Liu, D. et al. Black-carbon absorption enhancement in the atmosphere determined by particle mixing state. *Nat. Geosci.* **10**, 184–188 (2017).
11. Fierce, L. et al. Radiative absorption enhancements by black carbon controlled by particle-to-particle heterogeneity in composition. *Proc. Natl Acad. Sci.* **117**, 5196–5203 (2020).

12. Zhai, J. et al. Absorption enhancement of black carbon aerosols constrained by mixing-state heterogeneity. *Environ. Sci. Technol.* **56**, 1586–1593 (2022).

13. Wu, Y. et al. The role of biomass burning states in light absorption enhancement of carbonaceous aerosols. *Sci. Rep.* **10**, 1–10 (2020).

14. Romshoo, B. et al. Optical properties of coated black carbon aggregates: numerical simulations, radiative forcing estimates, and size-resolved parameterization scheme. *Atmos. Chem. Phys.* **21**, 12989–13010 (2021).

15. Romshoo, B. et al. Importance of size representation and morphology in modelling optical properties of black carbon: comparison between laboratory measurements and model simulations. *Atmos. Meas. Tech.* **15**, 6965–6989 (2022).

16. Smith, A. J. A. & Grainger, R. G. Simplifying the calculation of light scattering properties for black carbon fractal aggregates. *Atmos. Chem. Phys.* **14**, 7825–7836 (2014).

17. Liu, C., Xu, X., Yin, Y., Schnaiter, M. & Yung, Y. L. Black carbon aggregates: a database for optical properties. *J. Quant. Spectrosc. Radiat. Transf.* **222–223**, 170–179 (2019).

18. Tao, S. et al. Updated global black carbon emissions from 1960 to 2017: improvements, trends, and drivers. *Environ. Sci. Technol.* **55**, 7869–7879 (2021).

19. Fu, H. et al. Morphology, composition and mixing state of individual carbonaceous aerosol in urban Shanghai. *Atmos. Chem. Phys.* **12**, 693–707 (2012).

20. Bano, T. et al. Variation in aerosol black carbon concentration and its emission estimates at the mega-city Delhi. *Int. J. Remote Sens.* **32**, 6749–6764 (2011).

21. Hu, K. et al. Identifying the fraction of core-shell black carbon particles in a complex mixture to constrain the absorption enhancement by coatings. *Environ. Sci. Technol. Lett.* **9**, 272–279 (2022).

22. Brook, J. R. et al. Further interpretation of the acute effect of nitrogen dioxide observed in Canadian time-series studies. *J. Expo. Sci. Environ. Epidemiol.* **17**, 36–44 (2007).

23. Slater, J., Coe, H., Mcfiggans, G., Tonttila, J. & Romakkaniemi, S. The effect of BC on aerosol-boundary layer feedback: Potential implications for urban pollution episodes. *Atmos. Chem. Phys.* **22**, 2937–2953 (2022).

24. Raj, S. et al. Planetary boundary layer height modulates aerosol—water vapor interactions during winter in the megacity of Delhi. *J. Geophys. Res. Atmos* **126**, 24 (2021).

25. Samset, B. H. et al. Aerosol absorption: progress towards global and regional constraints. *Curr. Clim. Change Rep.* **4**, 65–83 (2018).

26. Ning, Z. et al. Black carbon mass size distributions of diesel exhaust and urban aerosols measured using differential mobility analyzer in tandem with Aethalometer. *Atmos. Environ.* **80**, 31–40 (2013).

27. Zhao, G. et al. Mixing state of black carbon at different atmospheres in north and southwest China. *Atmos. Chem. Phys.* **22**, 10861–10873 (2022).

28. Moteki, N. et al. Evolution of mixing state of black carbon particles: aircraft measurements over the western Pacific in March 2004. *Geophys. Res. Lett.* **34**, 11803 (2007).

29. Chen, X. et al. Quantifying evolution of soot mixing state from transboundary transport of biomass burning emissions. *iScience* **26**, 108125 (2023).

30. Wiedensohler, A. et al. Mobility particle size spectrometers: calibration procedures and measurement uncertainties. *Aerosol. Sci. Technol.* **52**, 146–164 (2018).

31. Savadkoohi, M. et al. The variability of mass concentrations and source apportionment analysis of equivalent black carbon across urban Europe. *Environ. Int.* **178**, 108081 (2023).

32. Cuesta-Mosquera, A. et al. Optical properties and simple forcing efficiency of the organic aerosols and black carbon emitted by residential wood burning in rural central Europe. *Atmos. Chem. Phys.* **24**, 2583–2605 (2024).

33. Gani, S. et al. Submicron aerosol composition in the world's most polluted megacity: the Delhi Aerosol Supersite study. *Atmos. Chem. Phys.* **19**, 6843–6859 (2019).

34. Mandariya, A. K. et al. Measurement report: hygroscopicity of size-selected aerosol particles in the heavily polluted urban atmosphere of Delhi: impacts of chloride aerosol. *Atmos. Chem. Phys.* **24**, 3627–3647 (2024).

35. Fountoukis, C. & Nenes, A. ISORROPIAII: a computationally efficient thermodynamic equilibrium model for K+-Ca2+-Mg2+-NH4+-Na+-SO42-NO3-Cl-H2O aerosols. *Atmos. Chem. Phys.* **7**, 4639–4659 (2007).

36. Kim, J. et al. Assessing optical properties and refractive index of combustion aerosol particles through combined experimental and modeling studies. *Aerosol. Sci. Technol.* **49**, 340–350 (2015).

37. Wozniak, M., Onofri, F. R. A., Barbosa, S., Yon, J. & Mroczka, J. Comparison of methods to derive morphological parameters of multi-fractal samples of particle aggregates from TEM images. *J. Aerosol. Sci.* **47**, 12–26 (2012).

38. Sorensen, C. M. Light scattering by fractal aggregates: a review. *Aerosol Sci. Technol.* **35**, 648–687 (2001).

39. Bond, T. C. & Bergstrom, R. W. Light absorption by carbonaceous particles: an investigative review. *Aerosol Sci. Technol.* **40**, 27–67 (2006).

40. Kahnert, M. On the discrepancy between modeled and measured mass absorption cross sections of light absorbing carbon aerosols. *Aerosol. Sci. Technol.* **44**, 453–460 (2010).

41. Wang, Y. et al. Fractal dimensions and mixing structures of soot particles during atmospheric processing. *Environ. Sci. Technol. Lett.* **4**, 487–493 (2017).

42. China, S., Mazzoleni, C., Gorkowski, K., Aiken, A. C. & Dubey, M. K. Morphology and mixing state of individual freshly emitted wildfire carbonaceous particles. *Nat. Commun.* **4**, (2013).

43. Zhang, Y. et al. Evidence of major secondary organic aerosol contribution to lensing effect black carbon absorption enhancement. *npj Clim. Atmos. Sci.* **1**, 1 (2018).

44. Bambha, R. P., Dansson, M. A., Schrader, P. E. & Michelsen, H. A. Effects of volatile coatings on the laser-induced incandescence of soot. *Appl. Phys. B Lasers Opt.* **112**, 343–358 (2013).

45. Luo, J. et al. Sensitivity analysis of morphology on radiative properties of soot aerosols. *Opt. Express* **26**, A420 (2018).

46. Kahnert, M. Optical properties of black carbon aerosols encapsulated in a shell of sulfate: comparison of the closed cell model with a coated aggregate model. *Opt. Express* **25**, 24579–24593 (2017).

47. Mackowski, D. W. & Mishchenko, M. I. A multiple sphere T-matrix Fortran code for use on parallel computer clusters. *J. Geophys. Res. Atmos.* **112**, 2182–2192 (2011).

48. Chen, L. et al. Cluster analysis of submicron particle number size distributions at the SORPES Station in the Yangtze River Delta of East China. *J. Geophys. Res. Atmos.* **126**, (2021).

49. Tunved, P., Cremer, R. S., Zieger, P. & Ström, J. Using correlations between observed equivalent black carbon and aerosol size distribution to derive size resolved BC mass concentration: a method applied on long-term observations performed at Zeppelin station, Ny-Ålesund, Svalbard. *Tellus B Chem. Phys. Meteorol.* **73**, 1–17 (2021).

50. Cheng, Y. H., Kao, Y. Y. & Liu, J. J. Correlations between black carbon mass and size-resolved particle number concentrations in the Taipei urban area: a five-year long-term observation. *Atmos. Pollut. Res.* **5**, 62–72 (2014).

51. Buonanno, G., Dell'Isola, M., Stabile, L. & Viola, A. Uncertainty budget of the SMPS–APS system in the measurement of PM1, PM2.5, and PM10. *Aerosol. Sci. Technol.* **43**, 1130–1141 (2009).

52. Poulain, L. et al. Multi-year ACSM measurements at the central European research station Melpitz (Germany) – Part 1: Instrument robustness, quality assurance, and impact of upper size cutoff diameter. *Atmos. Meas. Tech.* **13**, 4973–4994 (2020).

Author contributions
BR together with TM, MLP, and AA conceptualized the study. AA and GH conducted the field observations in Delhi, with assistance from MVH, AWB, and MI. BR, AA and AKM conducted the data analysis. BR carried out the modeling experiments, with help from TM. MLP and TM validated the results and conclusions of the study. BR drafted the manuscript and created the figures and tables. All authors contributed to the scientific discussion and interpretation of the results as well as to the final manuscript writing.

Competing interests
The authors declare no competing interests.

Additional information
Supplementary information The online version contains supplementary material available at https://doi.org/10.1038/s41612-024-00634-0.

Correspondence and requests for materials should be addressed to Baseerat Romshoo.

Reprints and permissions information is available at http://www.nature.com/reprints

Publisher's note Springer Nature remains neutral with regard to jurisdictional claims in published maps and institutional affiliations.